Spring 2021

The field coupling mechanism study for near field probe

Shun Liu

Department:

THE FIELD COUPLING MECHANISM STUDY FOR NEAR FIELD PROBE

by

SHUN LIU

A THESIS

Presented to the Faculty of the Graduate School of the

MISSOURI UNIVERSITY OF SCIENCE AND TECHNOLOGY

In Partial Fulfillment of the Requirements for the Degree

MASTER OF SCIENCE IN ELECTRICAL ENGINEERING

2021

Approved by:

Dr. Chulsoon Hwang, Advisor
Dr. Daryl G. Beetner
Dr. DongHyun Kim

PUBLICATION THESIS OPTION

This thesis consists of the following paper formatted in the style used by the Missouri University of Science and Technology:

Paper I, found on pages 6–27, is intended for submission to *Transactions on Instrumentation and Measurement*.

ABSTRACT

In this part, the radius of the loop is used to predict the voltage induced by the E-field in the circular loop antenna. The thin rectangle loop and thick rectangle loop have been investigated. The equivalent radius of the rectangle loop is estimated by the average of the one over the distance between the points on the loop to the center of the loop. The estimation matches with the numerical simulation.

ACKNOWLEDGMENTS

First, I would like to express my sincere gratitude to my advisor, Dr. Chulsoon Hwang, for his support and guidance during my whole master's program. His invaluable advice and constant encouragement helped me overcome many difficulties. Then, I also want to thank Dr. Daryl G. Beetner and Dr. DongHyun Kim for helping in my research.

I also want to thank my family for encouraging and supporting me to continue studying, no matter if the results are good or bad. Additionally, I want to thank all members of the Electromagnetic Compatibility Laboratory of Missouri University of Science and Technology. Without their help, I could not have finished my research smoothly.

TABLE OF CONTENTS

LIST OF ILLUSTRATIONS

SECTION Page

PAPER I

LIST OF TABLES

PAPER I Page

1. INTRODUCTION

The E-field coupling of circular loop antenna has been analytically investigated in previous work [1-4]. However, for the near field probe, the rectangle loop aperture is easier to implement and control during the PCB fabrication. However, the rectangle loop does not have an analytical solution for the field coupling. In the first part, the equivalent radius of the rectangle is estimated by the averaged distance factor (one over the distance). Then, a simulation is swept to study the accuracy of the estimated equivalent radius. The comparison shows the prediction matches with the numerical simulation result. In the second part, a rejection improved probe design is proposed in that paper. The improved near-field probe has better rejection than the original design, and the coupling mechanism is investigated through the equivalent circuit.

2. EQUIVALENT RADIUS OF RECTANGLE LOOP

2.1. THIN RECTANGLE LOOP

Figure 2.1 shows the maximized E-field coupling direction for the loop antenna. Since the H-field does not penetrate the loop area, the coupling voltage does not include the H-field coupling. The voltage on the gap of the circular loop antenna induced by the incident E-field can be determined as [1]

$$V_E = j\omega\mu_0 bj\omega 2\varepsilon_0 b\pi E^i b. \quad (1)$$

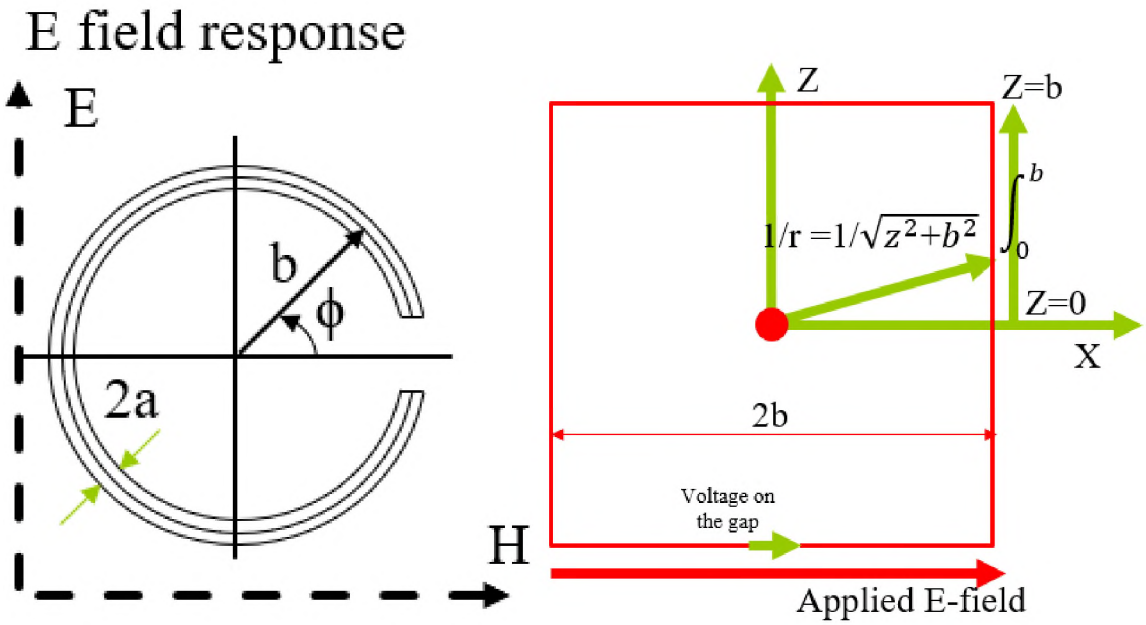

(a) (b)

Figure 2.1. Geometry of (a) classical circular loop (b) thin rectangle loop

For the rectangle loop, the equivalent radius is used to estimate the coupling. The equivalent radius of the rectangle loop can be estimated by the average of the integral of

one over distance from center to the wire center along the rectangle:

$$b' \approx \frac{1}{\frac{\int_0^b \frac{1}{\sqrt{z^2+b^2}}dz}{b}} \doteq b \ \ln(1+\sqrt{2}). \tag{2}$$

In Figure 2.2(b), the blue curve is the simulation result from the full-wave EM simulator [5], and the dashed red curve is a prediction based on the b' from the equation (2). The prediction matches with the simulation.

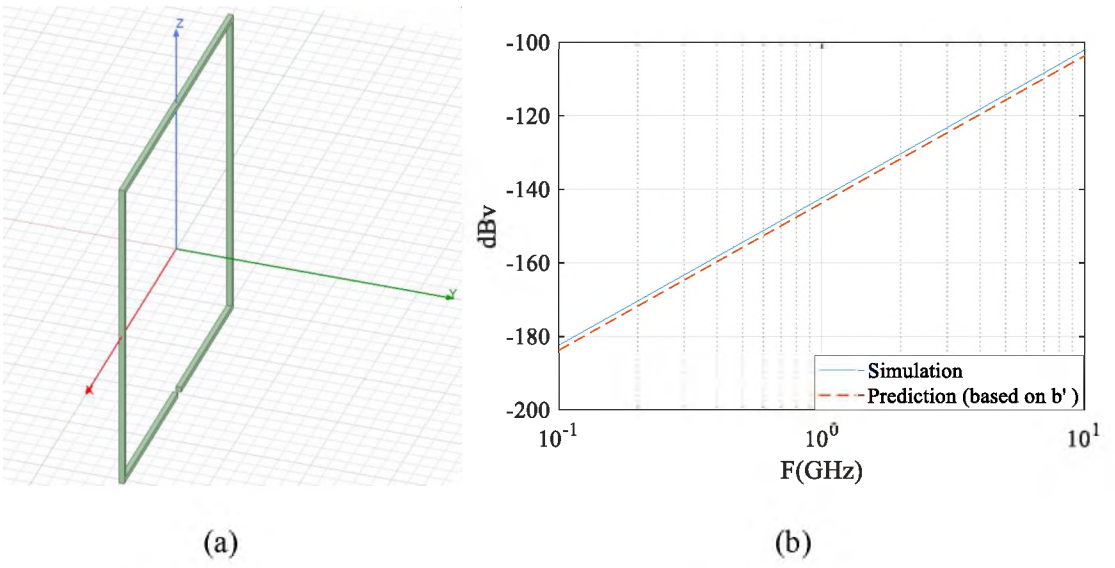

Figure 2.2. Thin rectangle loop (a) simulation model. (b) prediction and simulation

The prediction for E-field induced voltage on the gap (a=0.16mil, b=10mil) of the thin rectangle loop antenna matches with the numerical simulations. Then, sweep b from 1mil to 9mil, and the voltage induced on the gap is shown in Figure 2.3. As the a of b becomes larger, the match become less accurate. The estimation will be good for the thin rectangle loop antenna.

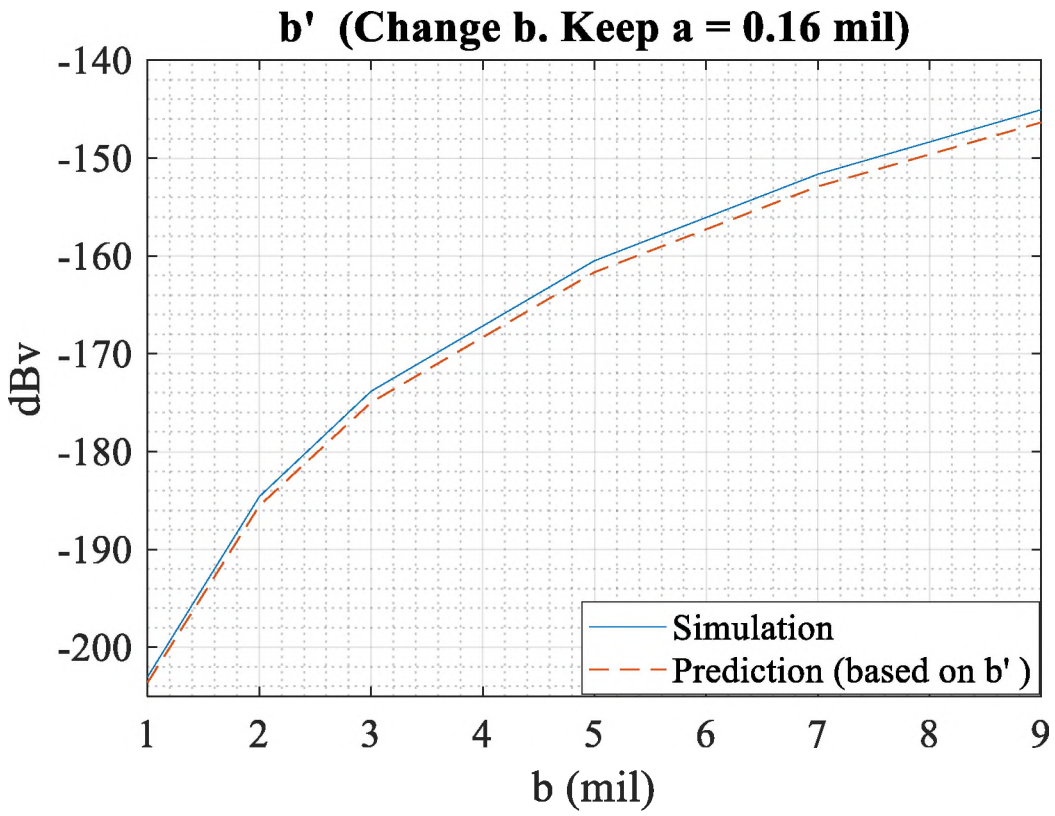

Figure 2.3. E-field induced voltage on the gap of thin rectangle loop (at 1GHz)

Figure 2.3 shows the result of sweeping the b and keep a as 0.16 mil in the simulation and the prediction from the equation (2). The voltage value from the simulation matches the prediction based on the b'.

2.2. THICK RECTANGLE LOOP

The equivalent radius of the thick rectangle loop can be estimated by the:

$$b' \approx \frac{1}{\frac{\int_{b-a}^{b+a}\frac{1}{x}dx}{2a}}? \ln(1+\sqrt{2}) \approx \frac{2a}{\log(\frac{b+a}{b-a})\ln(1+\sqrt{2})} \quad (3)$$

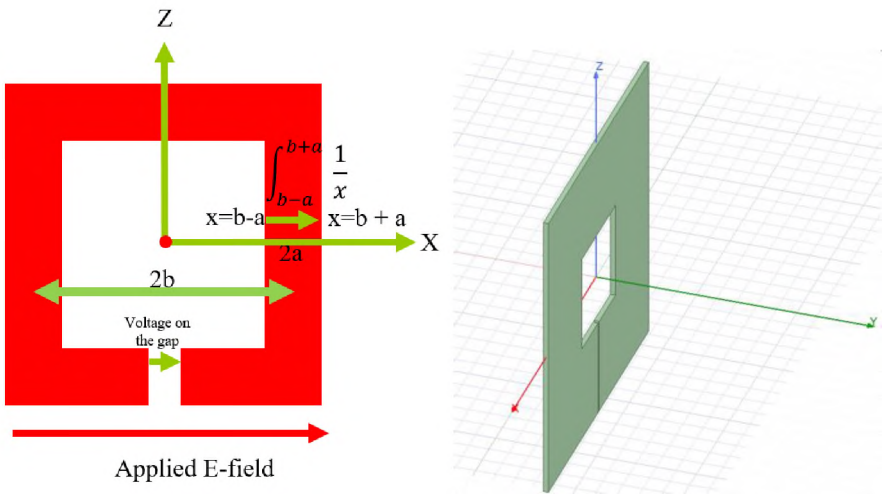

Figure 2.4. Thick rectangle loop (a) geometry (b) model in the numerical simulator

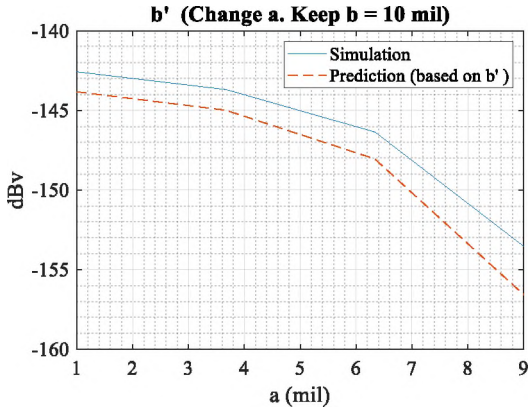

Figure 2.5. Prediction and simulation result

Figure 2.4 shows the geometry of the rectangle loop and the loop model in the simulation. In Figure 2.5, the simulation result from the numerical simulator matches the prediction for E-field induced voltage on the gap of thick rectangle loop based on equation (2).

PAPER

I. FIELD COUPLING MECHANISM OF MM-WAVE NEAR FIELD PROBE

ABSTRACT

The H-field and unwanted E-field coupling mechanism of the H-field probe is investigated and validated in this paper. This paper provides the precise field coupling model for the H-field probe to predict the voltage induced by the field. The thorough circuit model is based on the work that investigated the loop impedance model and the loop antenna's field response.

The full field response can be obtained in the form of a series expansion. This paper reveals that the zero-mode response corresponds to the H-field coupling, and the first mode corresponds to the E-field coupling. Since the working frequency range upper limit of purposed probe is around the first resonance, the equivalent model only includes the first mode and zero-mode. The predicted coupling by the equivalent circuit model matches with the numerical simulation and measurement result.

A novel shield structure is used to improve the probe's unwanted field rejection. The extension for the equivalent model also explains the improvement by the shield in the probe. The E-field rejection improvement is around 10dB up to 40GHz.

1. INTRODUCTION

Due to the development of the 5G wireless network, mm-wave frequency range has become relevant for electromagnetic interference (EMI) problems. To diagnosis and debugging those EMI issues, H-field probes are designed to visualize the near field of the DUT by measuring the electromagnetic fields from the DUT [1-5]. However, near-field probes covering the mm-wave frequency range are currently not available. The better sensitivity, spatial resolution, and rejection are the primary target for the probe design [6-10]. When the frequency goes higher, E-field coupling becomes more significantly compared to the H-field coupling and leads to erroneous data for the H-field measurement [7]. The E-field rejection is essential and challenging to achieve a high rejection value for a higher frequency. For probe design, it is essential to know which perimeter of the probe can determine the H-field sensitivity and E-field rejection. Many equivalent circuits are developed to describe the coupling of the probe and the Cal-kit in [8], [9], and [12]. Since those equivalent circuits use the mutual inductance between probe and Cal-kit to describe the coupling, they cannot directly describe the coupling between the probe and the incident field.

To directly describe the relationship between the probe's coupling voltage and the incident field, this paper proposed a field response equivalent circuit based on a well-known RLC form physical model of the circular loop antenna [12-17]. Figure 1(a) shows the classical circular loop antenna and Fid. 1(b) shows the geometry of the typical H-field probe. The numerical simulation results and the measurement results show the purposed equivalent circuit can accurately predict the H-field coupling and E-field coupling of the

circular loop antenna and the probe. The probe factor is used to describe the ratio between the electric or the magnetic field under test and the voltage induced at the probe. The probe factor is essential to know the field strength of the test device when using the probe in the near field measurement system. The field strength can be transformed by the measured output multiply the probe factor. Thus, the probe factor for H-field is defined as $PF_H = H / V_{Induced\_by\_H}(A^{-1}m^{-1}V^{-1})$. Probe factor for E-field is defined as $PF_E = E / V_{Induced\_by\_E}(m^{-1})$.

The probe factor is characterized in the measurement with the two-step procedure [8-11]. First, use the H probe to scan above the Cal-kit trace and get max H-field coupling. Second, rotates the H probe 90 degrees and scan above the Cal-kit to get the max E-field coupling. Probe rejection is determined as V_{Hmax} / V_{Emax}.

In Section 2, the physical-based equivalent circuit is developed and validated with the full-wave EM numerical simulator [18]. In Section 3, we designed the ultra-wideband H-probe for 1-40GHz and built the physical-based equivalent circuit corresponding to the probe. The measured PFH matches with the prediction of the equivalent circuit. In Section 4, the equivalent circuit is used to predict the E-field coupling. The prediction for E-field coupling matches with the measurement result. In Section 5, a novel structure similar to the handmade structure in [8] is implemented in the probe during the printed circuit board (PCB) fabrication process. The measured rejection is above 15dB for 1-20GHz and 10 dB for 20-40GHz. The rejection improvement is around 10dB for 20-40GHz compared to the original design.

2. THEORY OF FIELD COUPLING IN THE LOOP ANTENNA

2.1. RLC MODEL OF CIRCULAR LOOP ANTENNA

The proper RLC model of the circular loop antenna is transformed from the input impedance function of the circular loop antenna by Arnold [12]. The input impedance of loop antenna follows by definition:

$$Z_{in} = \frac{1}{(\frac{1}{Z_0} + \sum_{m=1}^{\infty} \frac{1}{Z_m})} \quad (1)$$

Each series modal impedance is given by

$$Z_0 = j\pi\xi_0 a_0 = R_0 + j\omega L_0 , \quad (2)$$

$$Z_m = j\pi\xi_0 a_m / 2 = R_m + j(\omega L_m - \frac{1}{\omega C_m}) , \quad (3)$$

where a_m , R_m , C_m, and L_m are given in [12].

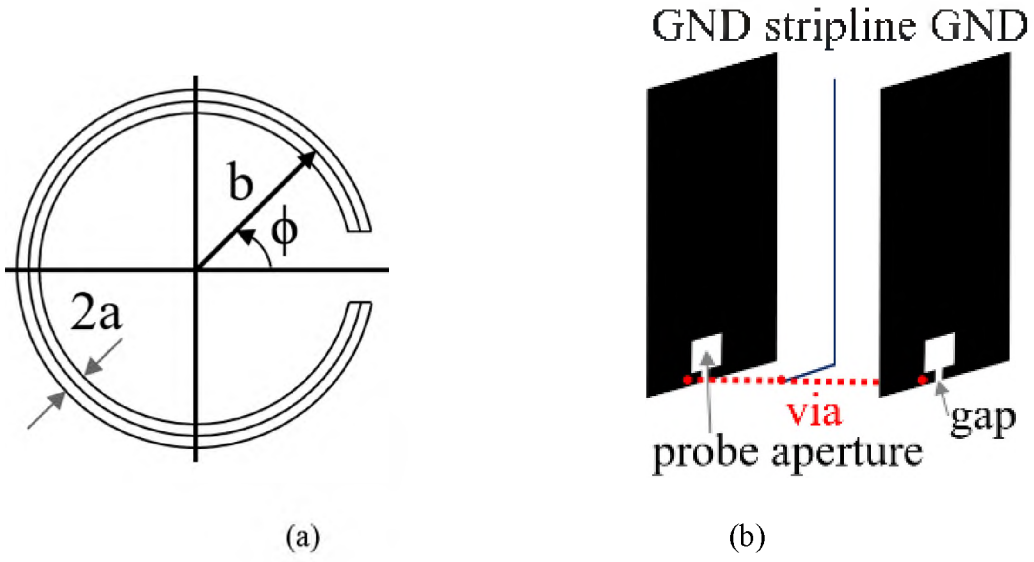

Figure 1. Antenna geometry (a) the classical loop (b) a typical H-field probe

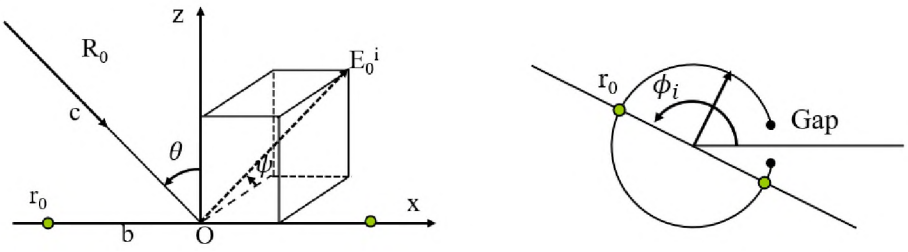

(a) (b)

Figure 2. Coordination (a) Plane-wave incident on a circular loop in the XY plane with center (0,0,0). (b) Projection of (a) onto the plane of the loop.

2.2. FIELD RECEPTION MODEL OF CIRCULAR LOOP ANTENNA

2.2.1. Field Response of Probe. The incident plane wave induces a voltage across the gap of the loop antenna. That is given in [14] as

$$V(Z_{Load}=\infty)=-E^{i}h_{e}(\theta,\phi_{i},\psi), \tag{4}$$

the effective antenna length (he) of the loop can be described by the infinite series as

$$h_{e}(\theta,\phi_{i},\psi)=2\pi b\frac{f_{0}a_{0}^{-1}+\sum_{m=1}^{\infty}f_{m}a_{m}^{-1}}{(a_{0}^{-1}+\sum_{m=1}^{\infty}a_{m}^{-1})}, \tag{5}$$

For an electrically small loop, zero-mode and first-mode can be a sufficiently good approximation

$$V=\sum_{n=0}^{\infty}V_{n},\ V_{n}=2\pi b\frac{f_{n}a_{n}^{-1}}{(a_{0}^{-1}+\sum_{m=1}^{\infty}a_{m}^{-1})}, \tag{6}$$

$$f_{0}=j\frac{\beta b}{2}(\sin\theta\cos\psi),\ f_{1}=\frac{1}{2}(\cos\theta\sin\phi_{i}\sin\psi+\cos\phi_{i}\cos\psi). \tag{7}$$

In Figure 3(c), the equivalent circuit shows a representation of Eq. (1) and Eq. (6).

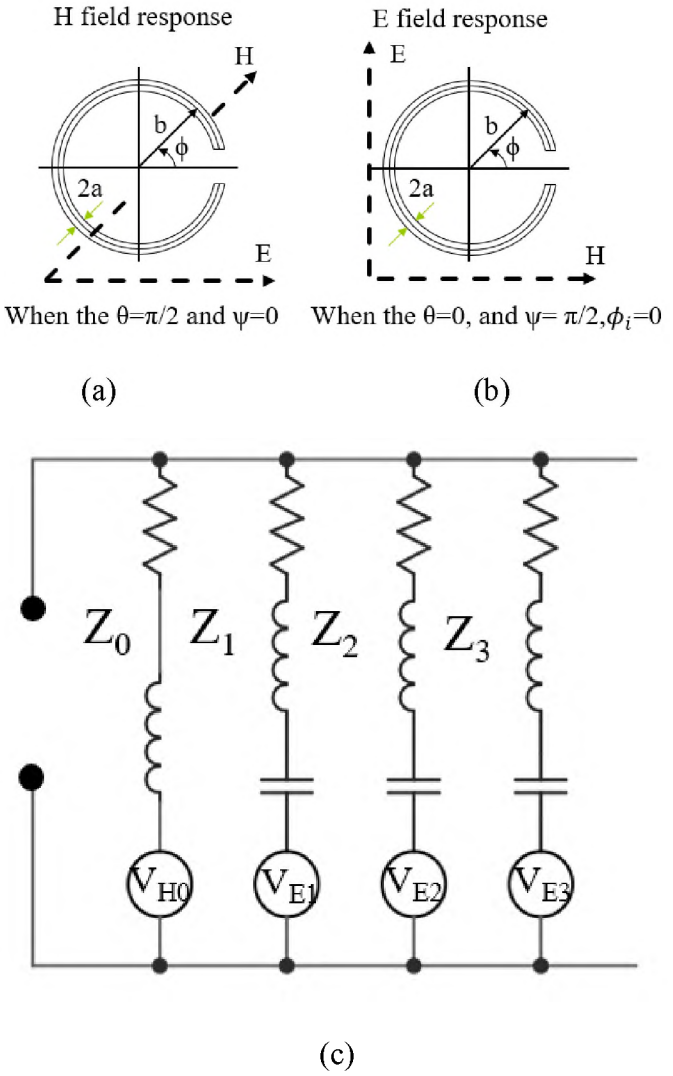

Figure 3. Field response (a) When the θ=π/2 and ψ=0. (b) When the θ=0, ϕi = π/2, ψ= π/2. (c) The field receiving model based on the RLC model of a circular loop antenna.

2.2.2. E-Field and H-Field Response. When the θ=π/2 and ψ=0, the H-field is perpendicular to the loop. Thus, the zero-mode comes from the H-field coupling. When the θ=0, ϕi = π/2, ψ= π/2, the H-field is in parallel with the loop plane and the E-field is in parallel with the loop gap. Thus, the first mode comes from the E-field coupling. The voltage of zero-order and first-order becomes

$$V_{H0} = j\omega\mu_0\pi b^2 H^i \sin\theta\cos\psi\,, \tag{8}$$

$$V_{E1} = \pi b E^i(\cos\theta\sin\phi_i\sin\psi + \cos\phi_i\cos\psi)\,. \tag{9}$$

The voltage across the reiver load resistance according to the circuit in Figure 3(c) is:

$$V_{rE} = V_{E1}\frac{(\frac{1}{\sum_{m=2}^{\infty}\frac{1}{j\omega C_m}} \| j\omega L_0 \| Z_{load})}{(\frac{1}{\sum_{m=2}^{\infty}\frac{1}{j\omega C_m}} \| j\omega L_0 \| Z_{load} + \frac{1}{j\omega C_1})}\,,$$

$$V_{rH} = V_{H0}\frac{(\frac{1}{\sum_{m=1}^{\infty}\frac{1}{j\omega C_m}} \| Z_{load})}{(\frac{1}{\sum_{m=1}^{\infty}\frac{1}{j\omega C_m}} \| Z_{load} + j\omega L_0)}\,. \tag{10}$$

$$V_{rE} = j\omega C_1 j\omega L_0 \pi b E^i\,,$$

$$V_{rH} = j\omega\mu_0\pi b^2 H^i\,. \tag{11}$$

Eq. (8,9) clarifies the relation between field strength and voltage induced on the gap of the loop antenna. By assuming the directions of the H-field and E field as described in Figure 3(a) and (b), we have maximized field coupling represented in (11). According to the approximation Eq. (11),

The E-field coupling is proportional to the ω^2, which increases 20 dB faster than the H-field coupling. Figure 1(a) shows the typical geometry for the loop antenna. The loop antenna's b is ten mils, and the a is 0.16 mil. The loop size is close to the aperture of the purposed probe. In Figure 4, the predicted field response to the E-field and H-field of

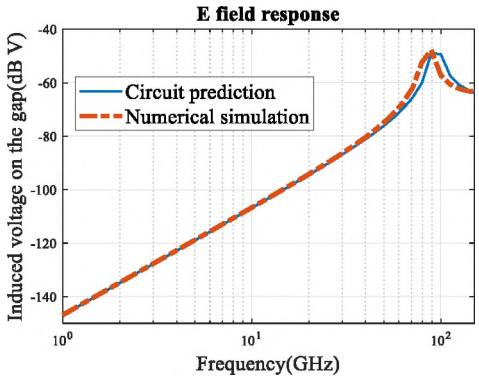

(a)

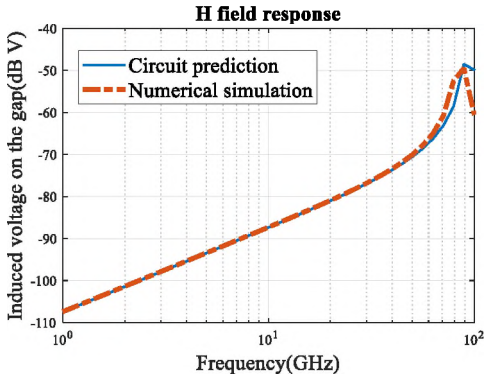

(b)

Figure 4. Field response from numerical simulation and purposed circuit. (a) E-field response. (b) H-field response. The proposed model can predict the field response up to 100GHz, which is far enough for the RFI problem investigation.

the loop antenna matches the field response in numerical simulation very well up to 100 GHz. According to the numerical simulation result and the circuit prediction, the E-field coupling increases around 40dB per decade, while the H-field increases by 20 dB per decade. Thus, the E-field coupling is more significant than H-field coupling at higher frequencies, which would create extensive erroneous data for the H-field measurement. This behavior would be a big problem for the E-field suppression of the ultra-wideband H-field probe when the target is 1-40GHz.

3. H-FIELD COUPLING MECHANISM OF H PROBE

3.1. PROBE DESIGN

Figure 5(a) shows the geometry of the purposed magnetic field probe. The probe is designed as three layers to maintain symmetry stack up. The probe was designed in the numerical software HFSS first and built by the fabrication house.

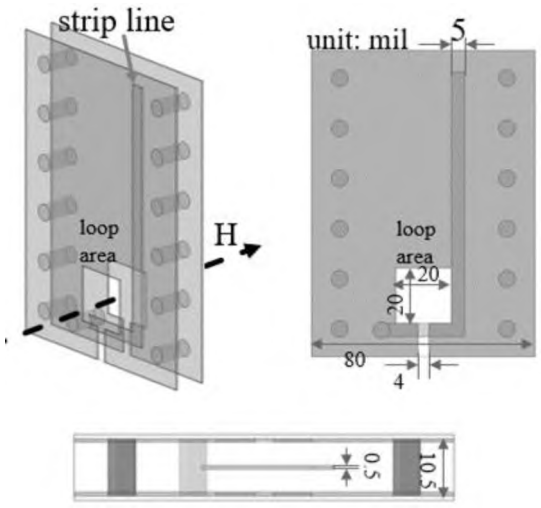

(a)

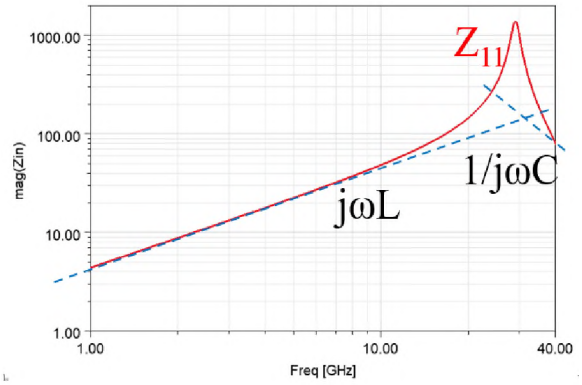

(b)

Figure 5. Probe (a) Geometry (b) Z_{11}: Input impedance looking into the probe.

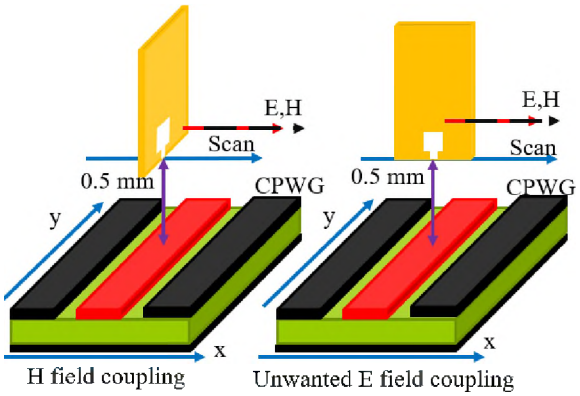

(a)

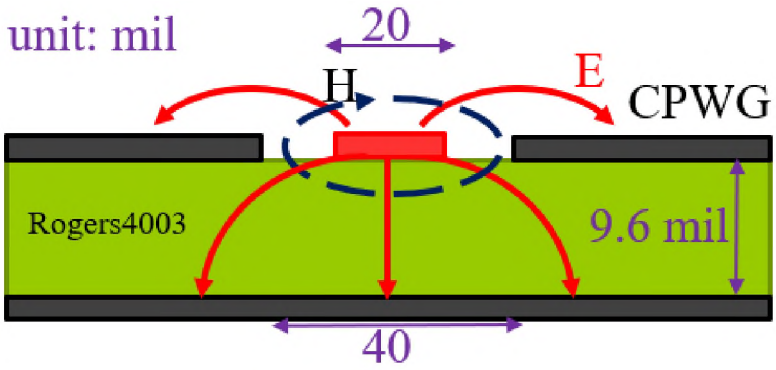

(b)

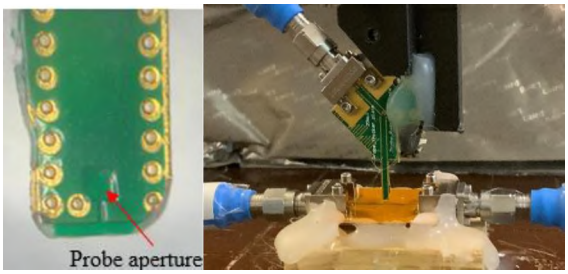

(c)

Figure 6. Probe setup (a) Measurement setup for E- and H-field coupling to the H-field probe. (b) Cal-kit coplanar waveguide geometry (CPWG). (c) Probe tip of the fabricated probe prototype.

The input impedance looking into the probe extracted from the numerical simulation can be model as the L and C_{total} in parallel. The L and C total extracted from

the Z input impedance are listed in the Table 1. According to [12], C1 is approximate as half of C total. The H-field coupling is modeled as the voltage source in the zero-order branch induced by magnetic flux change. The voltage magnitude depends on the open area in the probe.

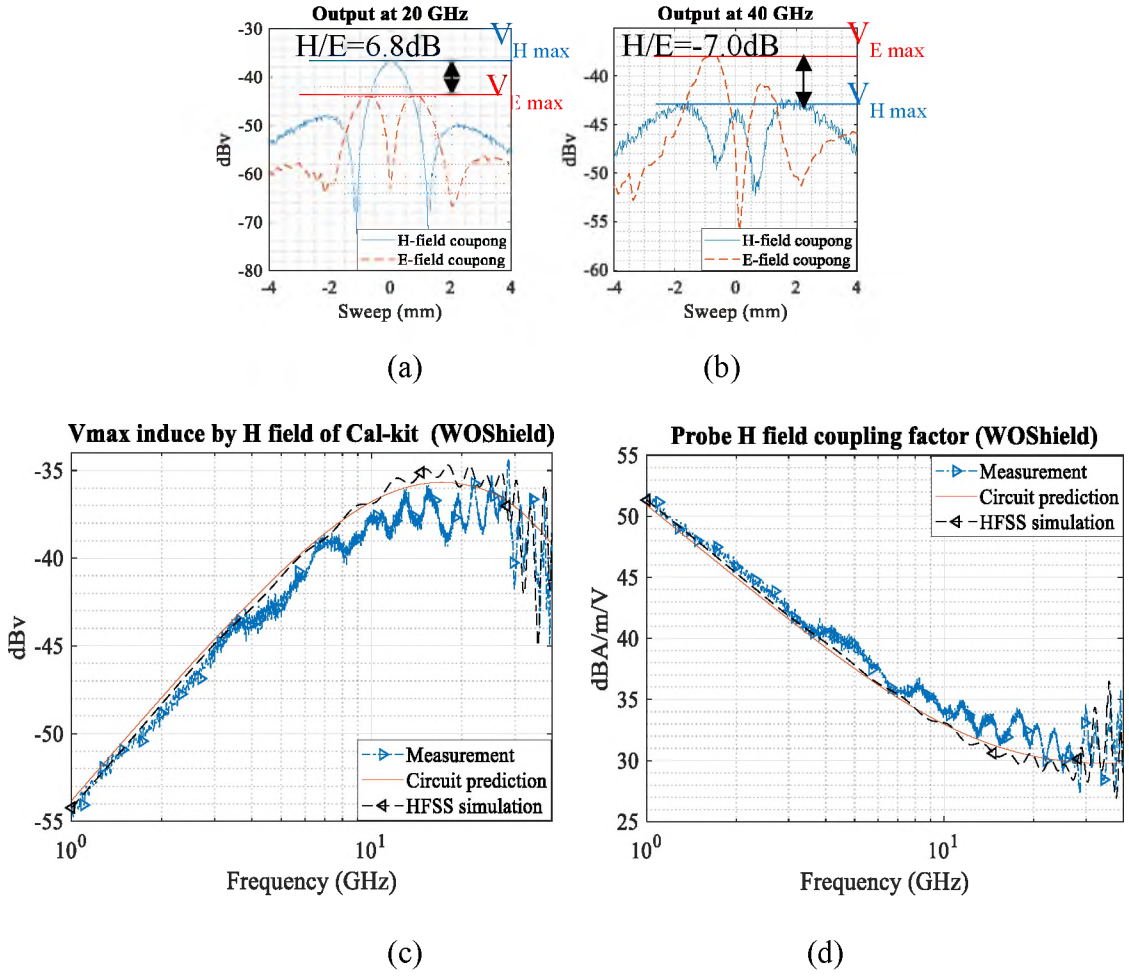

Figure 7. Measurement result (a) H-field and E-field induced voltage output during the scanning (0.5mm above the trace) at 20GHz. Rejection is defined as V_{Hmax}/ V_{Emax}. (b) H-field and E-field induced voltage output during the scanning (0.5mm above the trace) at 40GHz. (c) Measured, predicted, and simulated voltage induced by the H-field (1GHz-40GHz). (d) PF_H (A/m/V) from (1GHz-40GHz). The H-field magnitude is extracted from the numerical simulation. The characterization process has been detailly described in [10].

3.2. PF_H OF H PROBE

In the equivalent circuit, the small R and L in series with the capacitance in the impedance model of the loop antenna can be ignored. The probe factor is expressed as:

$$PF_H = \frac{H^i}{V_{rH}} = \frac{(\frac{1}{\sum_{m=1}^{\infty}\frac{1}{j\omega C_m}} \| Z_{load} + j\omega L_0)}{j\omega\mu_0 S(\frac{1}{\sum_{m=1}^{\infty}\frac{1}{j\omega C_m}} \| Z_{load})}, \quad (12)$$

Figure 7(a) shows a good match between the voltage induced in the probe from the numerical simulation, circuit prediction, and measurement result. The change of H-field induces the electromotive force as jwμSH. Thus, the measured probe factor of H-field rises around 20dB per decade, which fits with the circuit prediction. Since Z load is 50ohm, the Probe factor cannot maintain 20dB per decade for higher frequency. The discrepancy between the theory and numerical simulation results is negligible. The fabricated probe with long stripline shows multiple resonances in the measurement result due to the impedance mismatch for the high-frequency input.

Table 1. Original. Extracted L and C of Probe from Z11.

Symbol	Quantity	unit
L0	0.706	nH
C total =C1 + C2 + C3 +…	31.44	fF
C1	15.72	fF

4. UNWANTED E-FIELD COUPLING ANALYSIS

4.1. THE UNWANTED COUPLING MECHANISM IN THE PROBE

Based on the equivalent circuit in Figure 3(c), ignoring the small R and L in series with the capacitance in the impedance model of the loop antenna, the voltage induced by the E-field can be calculated as:

$$PF_E = \frac{E^i}{V_{rE}} = \pi h_e \frac{\left(\frac{1}{\sum_{m=2}^{\infty}\frac{1}{j\omega C_m}} \| j\omega L_0 \| Z_{load} + \frac{1}{j\omega C_1}\right)}{\left(\frac{1}{\sum_{m=2}^{\infty}\frac{1}{j\omega C_m}} \| j\omega L_0 \| Z_{load}\right)}, \quad (13)$$

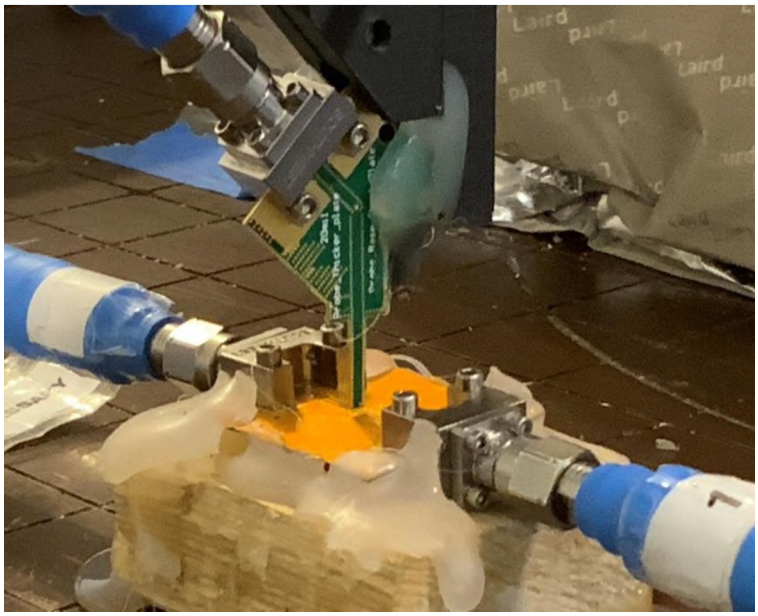

Figure 8. Cal-kit and the probe (after rotates 90°) placed above the Cal-kit.

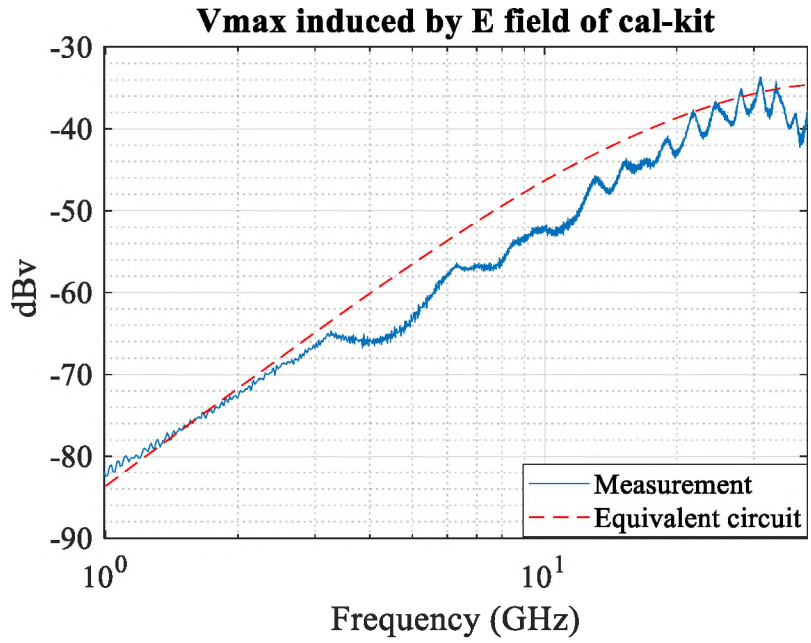

(a)

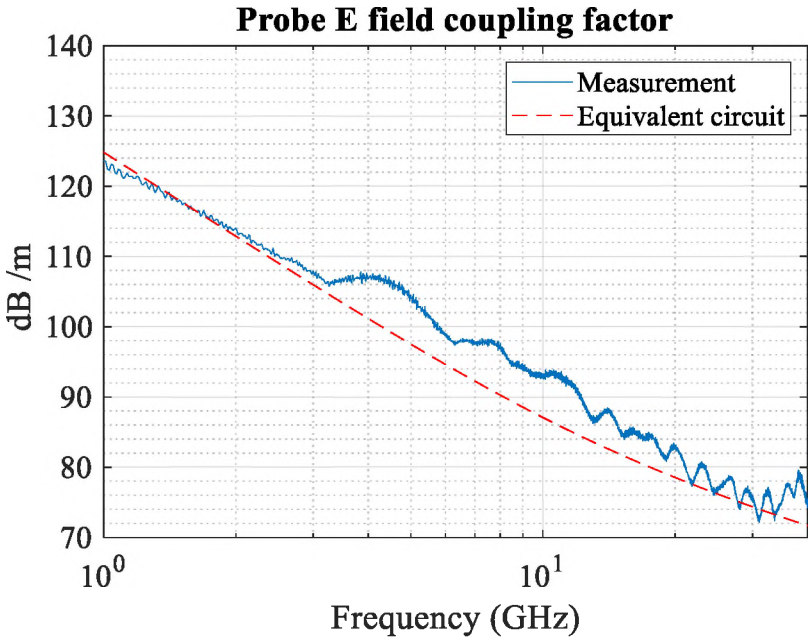

(b)

Figure 9. Measurement result (a) V max induced by E-field by circuit prediction (Equ.13) and measurement result. (b) PFE by circuit prediction and the measurement result. E-field strength is extracted by numerical simulation of Cal-kit.

When the E-field is parallel with the loop plane, the H-field does not penetrate the loop. The first to infinite orders correspond to the E-field coupling. According to (9), when the incident E-field is parallel with the loop plane, it gives the maximum coupling.

In the previous H-field case, the probe factor is 20dB per decade for the H-field coupling. However, the E-field coupling is 40dB per decade. Thus, due to the faster increase speed, the E-field coupling overrides the H-field coupling for higher frequencies.

4.2. MEASUREMENT RESULTS

The probe factor for the E-field is calculated as voltage output over the E-field strength $PF_E = E/V_E$. For the H probe, the smaller V_E means better rejection. Thus, PF_E should be as large as possible.

To characterize the PF_E, the probe rotates 90 degrees as showed in the Figure 8 after H-field characterization. Then the probe scans above the Cal-kit trace to get the maximum voltage induced by the E-field, and the field magnitude is extracted by the numerical simulation. The PF_E is defined as E field extracted from numerical simulation / $V_{\text{probe output induced by E}}$. Figure 9(a) shows a good match between the voltage induced in the probe from the circuit prediction and measurement result. The measured probe factor of E-field increases around 40dB per decade, which fits with the circuit prediction as Eq. (13). Figure 9 (b) shows a good match between the PF_E from the circuit prediction and measurement result. Thus, this equivalent circuit can predict the H-field and the E-field coupling accurately.

5. REJECTION IMPROVEMENT METHOD

A novel copper plate structure similar to the structure in the paper [8] under the probe is added during the fabrication process to improve the rejection of the probe.

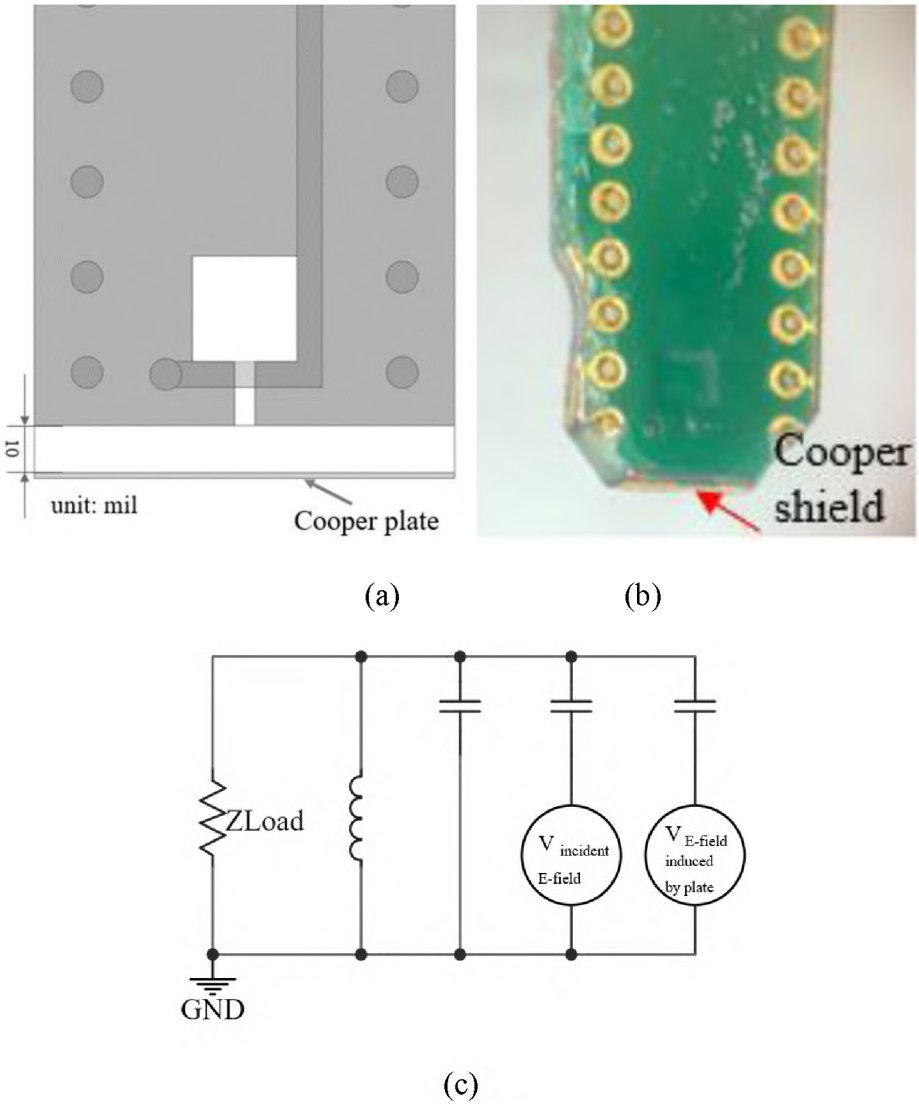

Figure 10. Probe with copper shield (a) A copper plate on the bottom of the probe. (b) This copper plate was added to the bottom edge of the PCB by the edge plating process in the fabrication. (c) This copper plate induces the capacitance between shield and loop. Since the shield induces the reverse E-field due to the incident field, the coupling from the shield is modeled as a reverse voltage source.

5.1. THE REJECTION OF PROBE

In [8-9], the rejection is defined as the ratio between max E-field coupling and the max H-field coupling. The rejection can be expressed as

$$RE_{Hmax/Emax} = \frac{V_{Hmax}}{V_{Emax}}. \tag{14}$$

$$RE_{Hmax/Emax} = \frac{PF_H H_{max\_field\_of\_Cal-kit}}{PF_E E_{max\_field\_of\_Cal-kit}}. \tag{15}$$

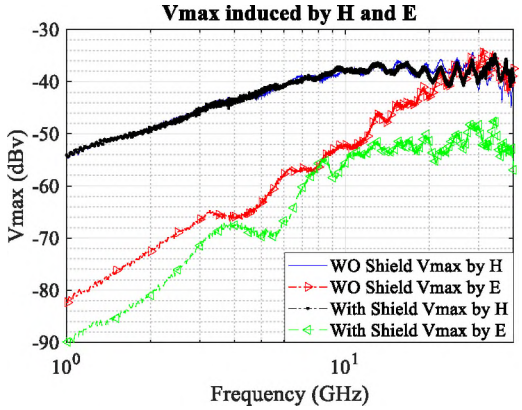

(a)

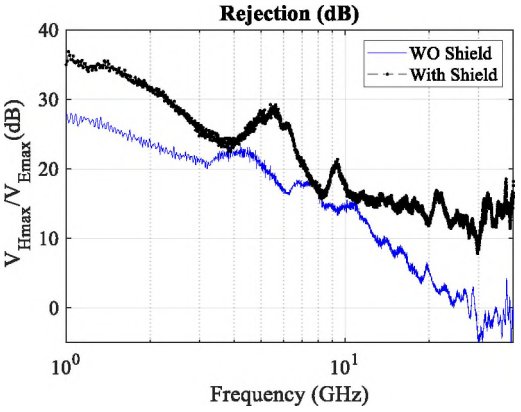

(b)

Figure 11. (a) Measured Vmax by H and E of the probe with/without shield. The unwanted E-field is minimized by the shield plate added in the fabrication (b) Rejection of with/without shield

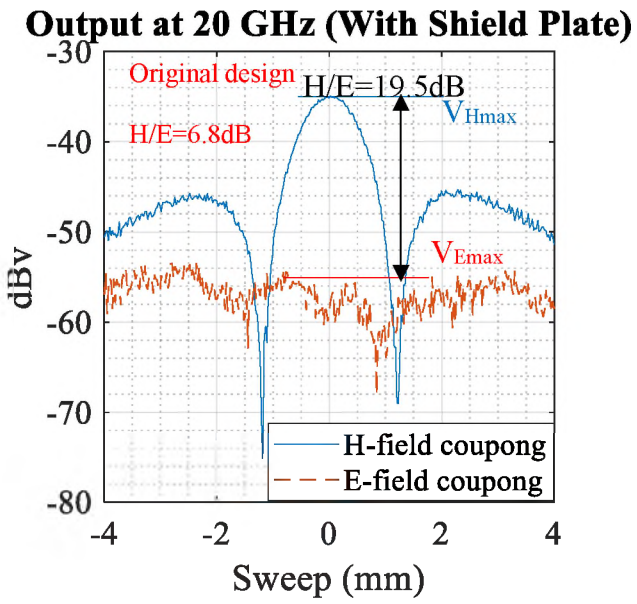

(a)

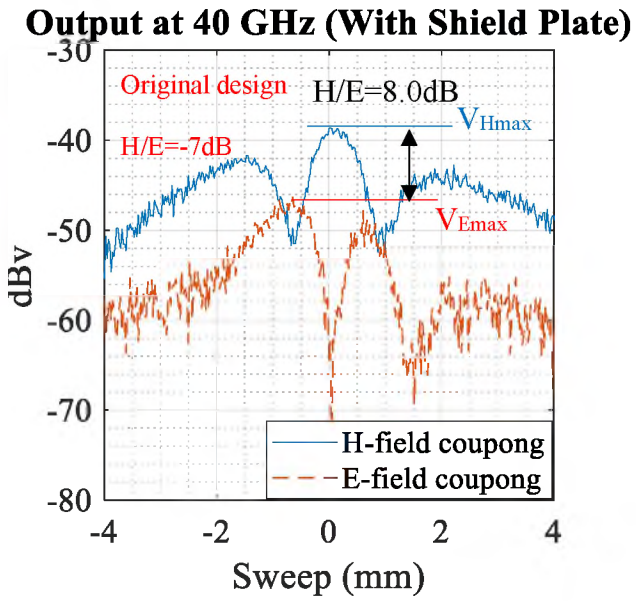

(b)

Figure 12. Measurement result (a) With shield probe scanned above the Cal-kit at 20GHz. (b) With shield probe scanned above the Cal-kit at 40GHz.

This rejection definition is based on the probe factor of the probe and the field of DUT, which will not only depend on the probe. The rejection calibration needs to rotate

the probe by 90 degrees after H-field calibration and scan above the trace to get the max output induced by E-field [8].

5.2. SUPPRESSION PLATE CIRCUIT EXPLANATION

When the incident field is impinging onto the shield, the shield will induce a reverse E-field compared to the incident field. Thus, this reverse E-field induced by the shield can minimize the E-field coupling of the probe. That reverse E-field also induces the voltage on the load of probe. Compare to the probe without additional shield plate, the improvement is depending on the coupling from the additional shield plate. Thus, the voltage on the gap of the probe can be expressed as $V_{E\ without\ shield} = V_E\ j\omega C_1 j\omega L$, and $V_{E\ shield} = V_E\ j\omega C_1\ j\omega L - V_{E\ shield}\ j\omega C_{shield}\ j\omega L = (V_E C_1 - V_{E\ shield} C_{shield})\ j\omega j\omega L$.

Thus, the shield only changes the coupling magnitude and will not change the frequency dependency. Fig. 8(c) shows the corresponding equivalent circuit. Fig. 8(d) shows the E field coupling after added the shield plate from the simulation. The coupling after added the shield plate is still rising at the rate of 40dB per decade of frequency, which fit the expectation.

5.3. MEASUREMENT RESULTS

The floating plate is on the bottom of the probe. Figure 10(a) shows that the E-field coupling is minimized in the whole frequency range. The voltage induced by the H-field is 10dB higher than the voltage induced by the E-field at 40GHz for the shielded probe, and the influence of the shield on the H-field coupling is negligible. During the

probe design, the equivalent circuit successfully predicts the improvement and guides the design process.

The modified probe is characterized with the same measurement setup described in Section3 and Section4. The measurement results are shown in Figure11 and Figure12. Figure 11(a) shows that the E-field coupling is minimized in the whole frequency range. The voltage induced by the H-field is 10dB higher than the voltage induced by the E-field at 40GHz for the shielded probe, and the influence of the shield on the H-field coupling is negligible. The rejection is 8 dB at 40G Hz and 19.5dB at 20 GHz, comparing to -7 dB at 40 GHz and 6.8 dB at 20 GHz in the previous design.

6. CONCLUSION

The purposed physical-based equivalent circuit directly described the field response of the probe accurately, applicable for the mm-wave frequency range. It provides a way to calculate and understand the probe factor and rejection of the probe easily. According to the analytical analysis, the E-field coupling rises around 40 dB per decade, but the H-field coupling only rises around 20 dB per decade. Thus, it is very crucial to improve the rejection for the higher frequency. The equivalent circuit helped in the design process and explained the rejection improvement mechanism. The measurement results have shown that the H and E-field coupling can be predicted by the equivalent circuit and the rejection improvement result from the proposed method at 20GHz is 12.7dB and at 40GHz is 15dB.

REFERENCES

[1] Q. Huang, F. Zhang, T. Enomoto, J. Maeshima, K. Araki, and C. Hwang, "Physics-based dipole moment source reconstruction for RFI on a practical cellphone," IEEE Trans. Electromagn. Compat., vol. 59, no. 6, pp. 1693–1700, Dec. 2017.

[2] Q. Huang et al., "MoM based current reconstruction using near-field scanning," in Proc. IEEE Int. Symp. Electromagn. Compat. Signal/Power Integr. (EMCSI), Washington, DC, USA, Aug. 2017, pp. 549–554.

[3] J. Zhang, K. W. Kam, J. Min, V. V. Khilkevich, D. Pommerenke, and J. Fan, "An effective method of probe calibration in phase-resolved near field scanning for EMI application," IEEE Trans. Instrum. Meas., vol. 62, no. 3, pp. 648–658, Mar. 2013.

[4] H. W. Ot, Electromagnetic Compatibility Engineering. New York, NY, USA: Wiley, 2009.

[5] D. Baudry, C. Arcambal, A. Louis, B. Mazari, and P. Eudeline, "Applications of the near-field techniques in EMC investigations," IEEE Trans. Electromagn. Compat., vol. 49, no. 3, pp. 485–493, Aug. 2007.

[6] H.-H. Chuang et al., "A magnetic-field resonant probe with enhanced sensitivity for RF interference applications," IEEE Trans. Electromagn. Compat., vol. 55, no. 6, pp. 991–998, Dec. 2013.

[7] Y. Xin, "Spatial resolution study for magnetic near-field probe," M.S. thesis, Missouri Univ. Sci. Technol., Rolla, MO, USA, 2018.

[8] S. Yang, Q. Huang, G. Li, R. Zoughi and D. J. Pommerenke, "Differential E-Field Coupling to Shielded H-field Probe in Near-Field Measurements and a Suppression Approach," in IEEE Transactions on Instrumentation and Measurement, vol. 67, no. 12, pp. 2872-2880, Dec. 2018, doi: 10.1109/TIM.2018.2831398.

[9] J. Bang, Y. Park, K. Jung and J. Choi, "A Compact Low-Cost Wideband Shielded-Loop Probe With Enhanced Performance for Magnetic Near-Field Measurements," in IEEE Transactions on Electromagnetic Compatibility, vol. 62, no. 5, pp. 1921-1928, Oct. 2020, doi: 10.1109/TEMC.2019.2946714.

[10] T. Dimitrijevic, A. Atanaskovic, N. S. Doncov, D. W. P. Thomas, C. Smartt, and M. H. Baharuddin, "Calibration of the Loop Probe for the Near-Field Measurement," 2019 European Microwave Conference in Central Europe (EuMCE), Prague, Czech Republic, 2019, pp. 567-570.

[11] Z. Yan, J. Wang, W. Zhang, Y. Wang, and J. Fan, "A simple miniature ultrawideband magnetic field probe design for magnetic near-field measurements," IEEE Trans. Antennas Propag., vol. 64, no. 12, pp. 5459–5465, Dec. 2016.

[12] A. F. McKinley, T. P. White, I. S. Maksymov, K. R. Catchpole, J. Appl. Phys.2012,112, 094911(1-9)

[13] E. Hallen, Nova Actae Regiae Soc.Sci. Ups. Ser. IV 11, 1 (1938).

[14] R. W. P. King, "The loop antenna for transmission and reception," in Antenna Theory, Part 1, Inter-University Electronic Series, Vol. 7, 1st ed., edited by R. E. Collin and F. J. Zucker (McGraw-Hill, New York, 1969),Chap. 11, pp. 458–482.

[15] C. F. M. Carobbi and L. M. Millanta, "Analysis of the common-mode rejection in the measurement and generation of magnetic fields using loop probes," IEEE Trans. Instrum. Meas., vol. 53, no. 2, pp. 514–523, Apr. 2004.

[16] C. F. M. Carobbi, L. M. Millanta and L. Chiosi, "The high-frequency behavior of the shield in the magnetic-field probes," IEEE International Symposium on Electromagnetic Compatibility. Symposium Record (Cat. No.00CH37016), Washington, DC, USA, 2000, pp. 35-40 vol.1, doi: 10.1109/ISEMC.2000.875533.

[17] C. Balanis, Antenna Theory: Analysis and Design, 3rd ed. (Wiley-Interscience,2005), p. 245.

[18] Ansys HFSS v2017.2, 2019. [Online]. Available: http://www.ansys.com

SECTION

3. CONCLUSIONS

In this topic, the equivalent radius of the loop antenna is studied in the first part. The estimation of the equivalent radius is extracted by the inverse of the average of the one over the radius. The numerical simulation shows the estimation for the equivalent radius is accurate. In the second part, the proposed physical-based equivalent circuit is developed to help the rejection improved design and explained the rejection improvement mechanism. The shield plate is added to the bottom of the probe during the fabrication process, and the measurement shows that the rejection improvement at 20/40GHz is up to 12.7/15dB.

BIBLIOGRAPHY

[1] C. F. M. Carobbi, L. M. Millanta and L. Chiosi, "The high-frequency behavior of the shield in the magnetic-field probes," IEEE International Symposium on Electromagnetic Compatibility. Symposium Record (Cat. No.00CH37016), Washington, DC, USA, 2000, pp. 35-40 vol.1, doi: 10.1109/ISEMC.2000.875533.

[2] R. W. P. King, "The loop antenna for transmission and reception," in Antenna Theory, Part 1, Inter-University Electronic Series, Vol. 7, 1st ed., edited by R. E. Collin and F. J. Zucker (McGraw-Hill, New York, 1969),Chap. 11, pp. 458–482.

[3] C. F. M. Carobbi and L. M. Millanta, "Analysis of the common-mode rejection in the measurement and generation of magnetic fields using loop probes," IEEE Trans. Instrum. Meas., vol. 53, no. 2, pp. 514–523, Apr. 2004.

[4] C. Balanis, Antenna Theory: Analysis and Design, 3rd ed. (Wiley-Interscience,2005), p. 245.

[5] Ansys HFSS v2017.2, 2019. [Online]. Available: http://www.ansys.com

VITA

Shun Liu received the B.E. degree in Opto-Electrical Information Science and Engineering from the Huazhong University Science and Technology, Wuhan, China, in 2018.

He received the Master of Science in Electrical Engineering from Missouri university of Science and Technology in May 2021.

His research interests included radio frequency interference, near-field probe, signal integrity, high-speed PCB design.